# A new mechanism for mineralizing systems based on cnoidal wave instabilities

**Chong Liu[1], Victor M. Calo[2], Lisa Tannock[3], Klaus Regenauer-Lieb[3,4], Manman Hu[1]**

[1]Department of Civil Engineering, The University of Hong Kong, Hong Kong, China
[2]School of Electrical Engineering, Computing and Mathematical Sciences, Curtin University, P.O. Box U1987, Perth, WA 6845, Australia
[3]School of Minerals and Energy Resources Engineering, UNSW, Sydney, NSW 2052, Australia
[4]WA School of Mines: Minerals, Energy and Chemical Engineering, Curtin, Bentley, WA 6102, Australia

**Key Points:**

- Cnoidal wave theory extends the fault-valve mechanism for geomaterials in compression;
- Replicating the mineralizing patterns allows assessing in-situ geological processes at the brittle-ductile transition;
- Numerical modeling allows inverting the stress state of compaction bands, rheological parameter, and the solid over fluid diffusion ratio.

Corresponding author: Manman Hu, mmhu@hku.hk

**Abstract**

The formation of mineral deposits in mesothermal quartz veins is a complex process that has been the subject of much research. The classical fault-valve hypothesis suggests that mineralization occurs when metamorphic fluids are injected during a brittle event and then locked in to mineralize, but this hypothesis does not fully explain the regular spacing of repeated mineralized patterns that are often observed. This paper proposes a new mechanism for mineralizing systems based on the theory of cnoidal waves in solids. Cnoidal waves are standing waves that can persist for long times in materials under compressive and extensional regimes. We investigate mineral deposits by analytical and numerical methods and show that the cnoidal wave instability theory provides a plausible alternative mechanism for mineralizing systems. This study opens a new avenue for field studies to demonstrate that the mechanism-based cnoidal waves play an essential role in the formation of mineral deposits.

## Plain Language Summary

Many major mineral deposits are found associated with quartz veins that have precipitated at around ∼300–400 °C located about ∼10 km deep, in fault systems subject to compression. Traditionally, mineralization in these tectonic setting has been thought to occur when fluids from mineral breakdown reactions are pumped under high pressure into the fault zone during earthquake cycles and left to precipitate in a fault valve. However, this theory is not compatible with our current understanding of fault mechanics in compressive environments and requires special pleading to explain the rhythmically repeated patterns of mineralization that are often seen. This paper proposes a new theory for mineralizing systems based on the theory of cnoidal waves in solids. Cnoidal waves are better known in fluids, where they are seen as strictly periodic stationary water waves in shallow water environments. Cnoidal waves can cause stress singularities in compressive and extensional stress regimes, forming mineral deposits. We employ numerical simulations to model the mineral deposit formation by cnoidal waves. The model reproduces natural mineralization patterns observed in the field. We conclude that the cnoidal wave instability theory provides a plausible new mechanism for mineralizing systems.

## 1 Introduction

A coupled hydro-chemo-mechanical process often forms mineralizing patterns in the brittle-ductile transition crust under high-temperature conditions. Understanding this process is vital for the mineral industry, as it can help predict mineral resource distribution. For example, orogenic gold deposits can be identified by their characteristic mineralizing patterns according to Tomkins (2013). Similarly, quantifying the spatial distribution of minerals can also be beneficial for ore processing (Barker et al., 2021; Liu et al., 2023a, 2023b). The coupled processes involved in mineralizing pattern formation include constituting elements of rock fracturing, fluid transport, dissolution, precipitation, mineral reactions, heat exchange and mineral crystallization. However, the details of how these ore-forming processes operate in the middle to upper crust are yet to be fully described and understood. A thorough understanding of fluid-rock interactions during rock deformation is of particular value for subsurface engineering applications, such as acidic-fluid injection activities and geothermal energy production (Späth et al., 2022; Tang & Hu, 2023; J. Chen et al., 2023).

Many gold-quartz vein arrays represent the uplifted roots of mineralizing systems from the mesothermal regime (∼300–400 °C) at around ∼10–15 km, which can be explained by the phenomenological fault-valve mechanism (Sibson et al., 1988). The fault-valve mechanism appeals to the conditions of the brittle-ductile transition where fluids released from metamorphic breakdown reaction from below the roots of the brittle fault system are pumped, under fluid pressures above the lithostatic, episodically into dilat-

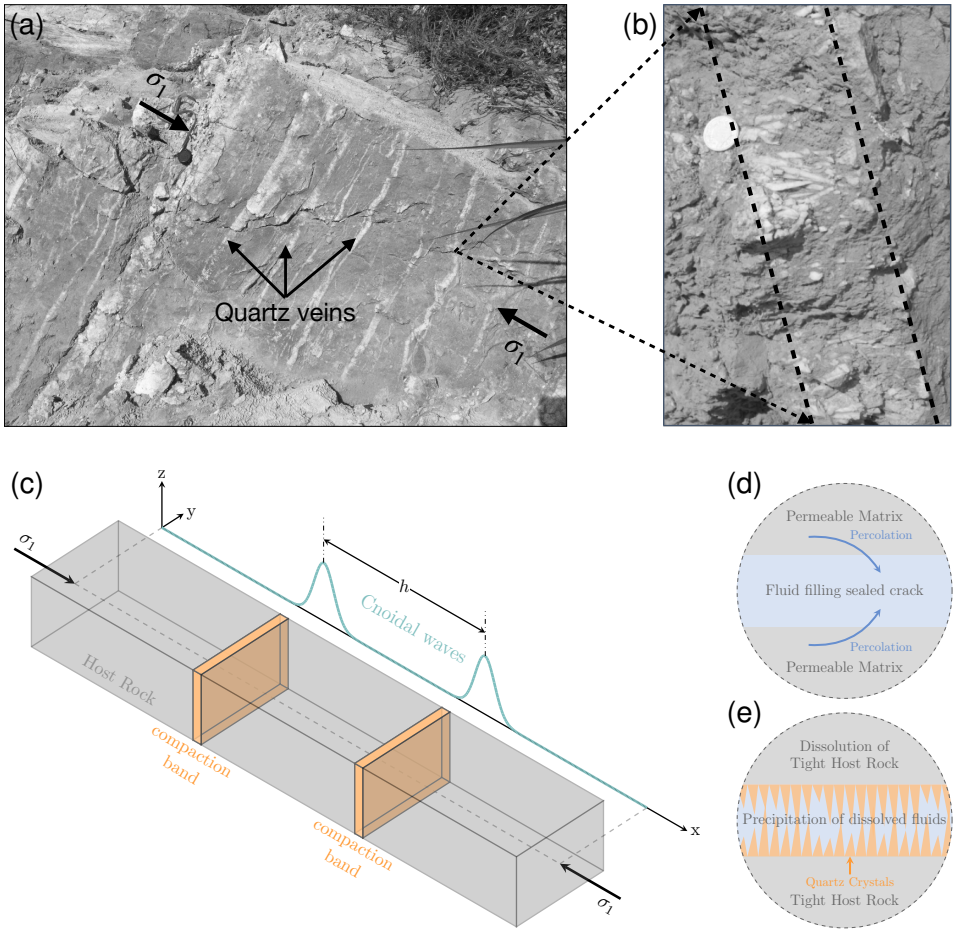


**Figure 1.** Rhythmic quartz veins in the Heyuan Fault, Guangdong Province, China: (a) macroscopic image for quartz veins taken near the Heyuan township, China, (b) close-up view of the quartz vein with idiomorphic, crystal-like quartz growth. Note that $\sigma_1$ in (a) denotes the normal component of the total stress. Two different settings for quartz vein formation, mineralization mainly occurs in the high-temperature regime. (c) the proposed cnoidal wave-driven fracturing mechanism; (d) crack-seal mechanism where brittle cracks open void space, creating lower pressures that attract mineralizing fluids through pressure solution or chemically induced mass transfer. Fluids percolate through the rock matrix and then precipitate in the open fractures. The mineral precipitates subsequently seal fractures (Ramsay, 1980; Bons et al., 2012); and (e) this study, high temperature ($> 300\,^{\circ}\mathrm{C}$) ductile equivalent of the fault-valve mechanism with nucleation of dilatant bands formed by cnoidal waves. The cnoidal wave mechanism provides a steady source of fluids on long geological time scales, allowing progressive chemical precipitation and syntaxial crystal growth from both sides of the fracture channel during a ductile process of continued compaction.

ing vein sets opening during seismic cycles. In the interseismic period, the fluids are effectively locked into the fault veins due to dilatancy-induced reduction in fluid pressures in the host rock and the subsequent mineral precipitates. This conceptual model was discussed in detail by (Hobbs & Ord, 2022, 2023) as the stress regime and the fault orientations are incompatible with the current understanding of fault mechanics in compressive tectonic regimes, and alternative solutions were sought. In this contribution, we fo-

cus on the geophysical modeling of the alternative geomechanical solution to allow the derivation of dynamic process parameters from the observed geological mineralization patterns. The detailed investigation of the geological implications will be the subject of a forthcoming contribution.

The problem addressed in this study is that the fault-valve model requires exceptional circumstances, such as the re-activation of an earlier normal fault as a non-optimally oriented thrust fault. The use of a Coulomb failure envelope in the original fault valve model also necessitates fluid stresses above the lithostatic stress. The alternative model (Hobbs & Ord, 2022, 2023) replaces the Coulomb envelope with a yield envelope that has a capped yield surface at higher pressure, which alleviates both the need for extremely high fluid pressures and supplying a consistent high angle of veins with respect to the direction of the maximum principal stress as observed in the field. The alternative model was a conceptual model that replaced the need for earthquakes with an oscillatory stress cycle in the aseismic field. In this work, we complete the conceptual model for mineralizing pattern formation using a physics-based approach simplified by assuming local equilibrium of mass exchange processes for dissolution-precipitation processes (Veveakis & Regenauer-Lieb, 2015; Alevizos et al., 2017). This simplifying assumption neglects stochastic processes at finer time-scales but allows analytical and numerical investigation of the observed patterns for inversion of dynamic properties under the assumption that they have reached a steady state. We use our approach to study quartz veins observed at the quartz reef in the Heyuan Fault, Guangdong Province, China. Figures 1(a-b) show macroscopic field images of quartz veins hosted in ultra-cataclasites, photographed in Heyuan, China (Tannock, Herwegh, Berger, Liu, Lanari, & Regenauer-Lieb, 2020).

## 2 Cnoidal Wave Theory

The counter-intuitive phenomenon (here, opening-model veins in compression) becomes plausible when we take the cnoidal wave theory in solids into account (Veveakis & Regenauer-Lieb, 2015). Cnoidal wave instabilities occur when the solid matrix's mechanical compaction rate outpaces the pore fluid's capability to diffuse out of the porous geomaterials. This situation occurs when the rate of fluid release reactions in a tight formation is pressure sensitive and triggered by a critical activation pressure (Alevizos et al., 2017). The activation threshold expresses the tight coupling between solid matrix deformation and fluid release reactions and may be understood as the physical micromechanism that corresponds to a capped yield envelope as fluid release reaction can trigger the onset of creep of the matrix. A brief summary of the derivation of the cnoidal wave equation can be found in Text S1 in Supporting Information.

The standing waves cause the rock to experience dilatant effects instead of compaction during stress concentration, forming dilatant compaction bands perpendicular to the maximum principal (compressive) stress. The solution is sign invariant and applies to the extensional regime with veins oriented at a small angle to the maximum principal stress direction. The conceptual model is a 1-D solution describing the competition between the characteristic length scales of diffusion of fluids from dissolution reactions and the diffusion of strain in the deforming solid matrix. The solution therefore needs to be interpreted along the opening axis of the veins. With this assumption it can incorporate shear deformation (Veveakis & Regenauer-Lieb, 2015; Regenauer-Lieb et al., 2016) and applies to the extensional and compactive shear bands while we restrict our investigation to purely compactive deformation for simplicity. We emphasize that the cnoidal wave theory is a nonlinear hydrodynamic approach and comes from a different perspective, which appears in opposition to the classical understanding of compaction bands, where grain crushing and pore collapse dominate in compression, resulting in lower permeable layers (Issen & Rudnicki, 2000). The apparent contradiction can nevertheless be reconciled if the crushed grains in the lower permeable layer are interpreted as a low viscosity fluid instead of a solid phase, which has been used to derive unknown pa-

rameters from field observations of conventional (crushed grain) compaction bands (Regenauer-Lieb et al., 2013).

The proposed theory has been used to explain several geological structures, such as fracturing network formation (Alevizos et al., 2017), Zebra dolomite banding (Kelka et al., 2017), shrinkage cracks (R. Chen et al., 2023), and melt segregation (Veveakis et al., 2014; Weinberg et al., 2015). Here, we will use the concept of cnoidal wave instabilities to explain the mechanism of mineralized patterns with an emphasize on quartz vein formation. Specifically, the induced dilatant compaction bands are interpreted as wave instabilities that can act as open fluid channels, trapping mineralized fluids, which leads to the crystallization and eventually development of mineralized patterns in rocks, as illustrated in Figures 1(c-e).

Although the solution is analytically tractable for integer power law coefficients of the matrix creep law, the cnoidal wave theory has a reputation for being difficult to solve numerically due to unbounded solutions (Veveakis & Regenauer-Lieb, 2015). Recently, a suitable method has been devised (Cier et al., 2021, 2022) allowing exploration of the entire parameter range. This study investigates the quartz vein formation by applying a robust numerical framework to solve the coupled cnoidal wave equations. Here, we quantitatively investigate the potential factors affecting the distance between quartz veins and provide new physical insights into the underlying mechanism. Additionally, we invert the geological parameters that are essential but difficult to constrain by replicating the quartz vein patterns observed in the field, such as solid viscosity, overstress, and rheology exponents in the nonlinear viscoplastic power laws.

## 3 Results

In order to explore the parameter space, we use a 1-D formulation for cnoidal waves based on the general theory of overstress plasticity (Perzyna, 1966) and mixture theory of poromechanics as follows (see Eq. (S10) and variables' and parameters' definition in Text S1 in Supporting Information),

$$\frac{\partial^2 \sigma}{\partial x^{*2}} - \lambda \sigma^m + \eta e^{\beta \sigma} = 0 \tag{1}$$

We solve (1) using an effective and robust discretization method called the adaptive stabilized finite element method (ASFEM), which captures the stress concentration phenomenon by automatically refining the mesh. The ASFEM overcomes the spurious oscillations of the classical FEM formulation for this highly nonlinear problem. For the detailed discretization scheme and the formulation for the ASFEM, the readers can refer to Cier et al. (2021). We use a FEniCS implementation of the method with constant coefficients for the third term of (1), which acts as a chemical regularization term (Alevizos et al., 2017). Hence, the material properties that scale the steady-state fluid pressure magnitude $\eta = 4.54 \times 10^{-9}$ and the chemo-mechanical activation term $\beta = 10$ are fixed. We adopt the symbol from Cier et al. (2021) by replacing $\sigma - 1$ with $u$ for numerical simplification to transfer inhomogeneous to homogeneous Dirichlet boundary conditions, although we impose the periodic boundary conditions at the two ends of the specimen. Also, initially, we fix the solid rheology's rate-dependent power law coefficient $m = 3$. The effect of changing material parameters will be addressed later.

### 3.1 The parameter $\lambda$ controls the visco-plastic instability

The poromechanical parameter $\lambda$ plays a crucial role in determining the profile of the normalized effective stress, including the number of stress singularities and distance between neighboring peaks. The physical meaning of $\lambda$ is the ratio of the mechanical deformation diffusivity over the internal fluid diffusivity, the loading rate over the diffusion rate of the pore fluid in (Veveakis & Regenauer-Lieb, 2015). The competition of the

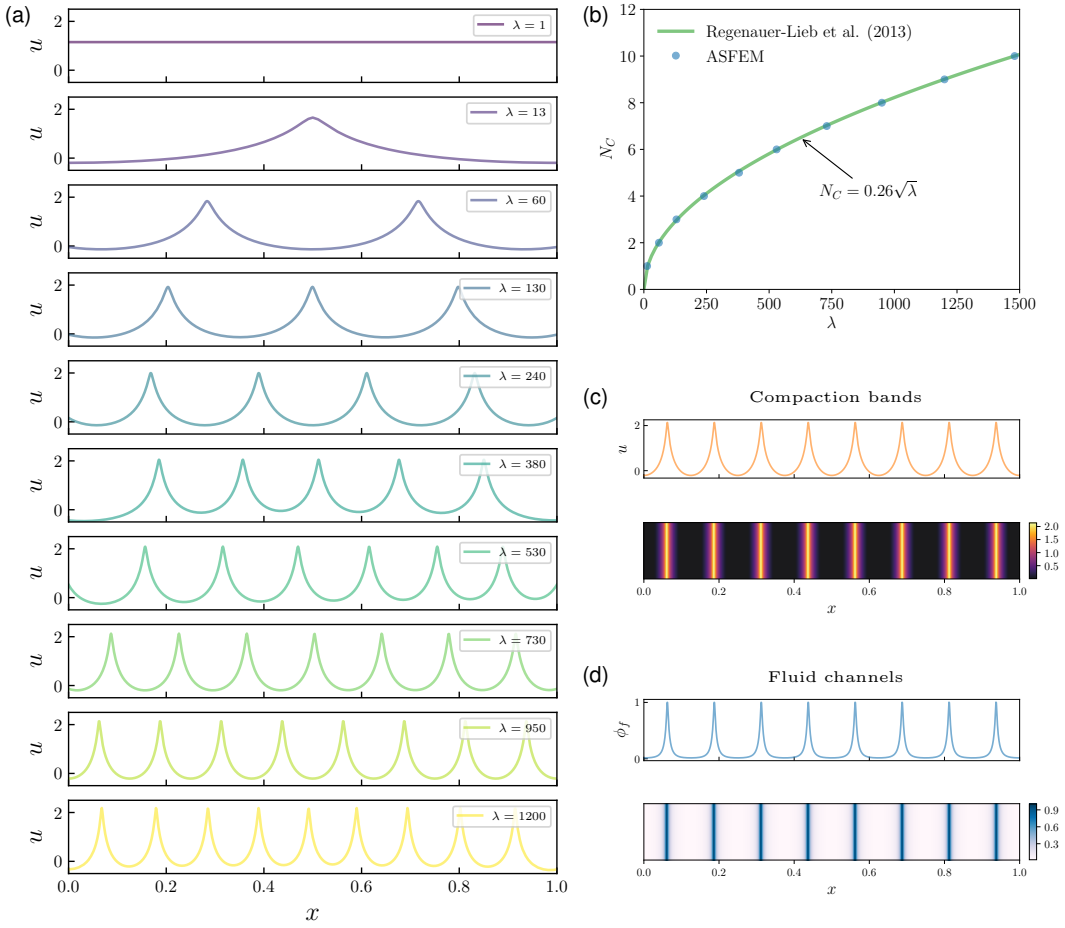


**Figure 2.** Effect of the diffusion ratio between solid and fluid phases $\lambda$: (a) stress profiles for varied $\lambda$ quantities; (b) agreement between the ASFEM simulations and analytical solutions of Regenauer-Lieb et al. (2013); (c) stress distribution and the corresponding compaction bands for eight peaks; and (d) the porosity increments and the possible fluid channels. Our 1-D simulations solve for 2-D compaction bands (c) and fluid pathways (d) for visualization.

above two processes governs the occurrence of volumetric instabilities. Taking two end-members, for example, we may expect a stable deformation when $\lambda \ll 1$, the fluid diffusion is much greater than the solid deformation, and the matrix has enough time to diffuse away any induced pore pressure by the mechanical loading rate. Conversely, wave instabilities may appear when $\lambda \gg 1$; in this extreme case, the rate of fluid transfer by the fluid diffusion process is much slower than the loading rate, which intensifies the fluid pressure on the first cnoidal compaction band. In the original analytical solution, the pressure goes to infinity. This instability can be controlled by the chosen regularization term for fluid pressure production (third term in (1)). Since the magnitude of the fluid pressure is unknown in the geological field example, and the style of the instability is unchanged, we focus on the investigation of the other parameters, e.g., $\lambda$ and $m$.

We use ASFEM to investigate the effect of the poromechanical parameter $\lambda$ on the appearance of the cnoidal wave instabilities. The lowest stress critical number for the emergence of the high fluid pressure is $\lambda_{crit} = 12.7$ as expected from the analytical solution without the regularization term. The compacted specimen displays multiple stress peaks when $\lambda > \lambda_{crit}$, while the perturbation will disappear if $\lambda$ is below this thresh-

old, see the $\lambda = 1$ case in Figure 2(a). We compare several numerical simulations for the critical $\lambda$ to different stress peaks to validate our simulator, as Figure 2(a) shows. The initial perturbation can evolve into multiple peaks as the $\lambda$ values grow, which matches well with the empirical relationship $N_C = 0.26\sqrt{\lambda}$ based on theoretical analysis as Figure 2(b) shows. Solutions with a higher number of stress peaks can only be resolved numerically when the wavelength of the initial perturbation is increased along with $\lambda$. Figures S1–S2 in Supporting Information plot the initial perturbation for different cases by adjusting the constant $s$ in (S11) and how the perturbation evolves and separates to five peaks at five iterations. Figure 2(c) illustrates stress peak numbers $N_C = 8$ periodically placed in the specimen, in which the contours are the extension of the 1-D simulations for visualization of the potential compaction bands, and the curves give the stress profiles. In summary, the parameter $\lambda$ controls the number of stress peaks and the distance between them. Therefore, we expect specific $\lambda$ values to describe specific configuration patterns of compaction bands in the field.

### 3.2 Porosity enhancement indicating fluid channels

A significant porosity enhancement occurs with the stress singularities, appearing as channel instabilities. We adopt the formulation of porosity evolution during the fluid-releasing metamorphic reaction Eq. (S2) from Alevizos et al. (2017) as:

$$\phi_f = \phi_0 + \Delta\phi_{\text{mech}} = \phi_0 + (1 - \phi_0)\sigma'^m \dot{\varepsilon}_n \Delta t \tag{2}$$

with $\phi_0$ is the initial volume fraction of fluid with a negligible value of 0.1% (Veveakis & Regenauer-Lieb, 2015). The mechanically induced porosity change $\Delta\phi_{\text{mech}}$ results from the irreversible viscoplastic stress acting on the solid phase over a reference time interval $\Delta t$. Figure 2(d) presents the volume fraction of fluid phase calculated by (2) for the case of $N_C = 8$. Again, we plot the contour to illustrate the potential fluid pathways corresponding to the compaction bands. The high porosity areas correspond to the stress singularities, indicating that the porosity change depends on the third term in (1) regularizing the fluid production term. In the extreme case (i.e., the regularizing term is set to zero), the stress singularities approach infinity ($\sigma' \to \infty$), and the porosity tends to reach its maximum value of one ($\phi_f \to 1$), creating fluid channels. Thus, we emphasize that local porosity enhancement can occur for both signs of volumetric strain (in extension and compressive environments), leading to fluid channels with high porosity.

### 3.3 Inverting the diffusivity ratio for quartz veins

We investigate the application shown in Figure 1 to test whether the cnoidal wave hypothesis can explain the periodic mineralized pattern formation in compression, in a compressive regime, within the brittle-ductile region. Thus, we use the proposed wave-driven pattern formation to invert for $\lambda$, i.e., the ratio of the diffusion of mechanical deformation over the diffusion of the fluid species. First, we observe that quartz veins resemble periodic patterns generated by cnoidal waves in Figure 3(a). This similarity shows that it is possible to explain the emergence of quartz veins due to the stress singularities by the cnoidal waves as shown in Figure 1(c). The volumetric instabilities produce rhythmically spaced open channels (fractures). Synchronously, the surrounding pore fluid in the matrix tends to infiltrate into the newly generated channels, which forms the fluid paths for mineral transport as depicted by Figure 1(d). Consequently, the dissolved silica is transported by fluid flow and may precipitate along the interface across the matrix and the formed channels (fracture walls), forming the quartz veins with quartz crystals growing in the direction of vein opening (syntaxial growth) (Bons et al., 2012) as sketched in Figure 1(e). Since the instability presented is a steady-state solution, the cnoidal wave instabilities provide both the sudden initial vein opening mechanism at the critical $\lambda$ and the steady supply of new quartz-saturated fluids during the crystallization of the elongate, blocky to needle-like quartz crystals. The synchronous growth of vein aper-

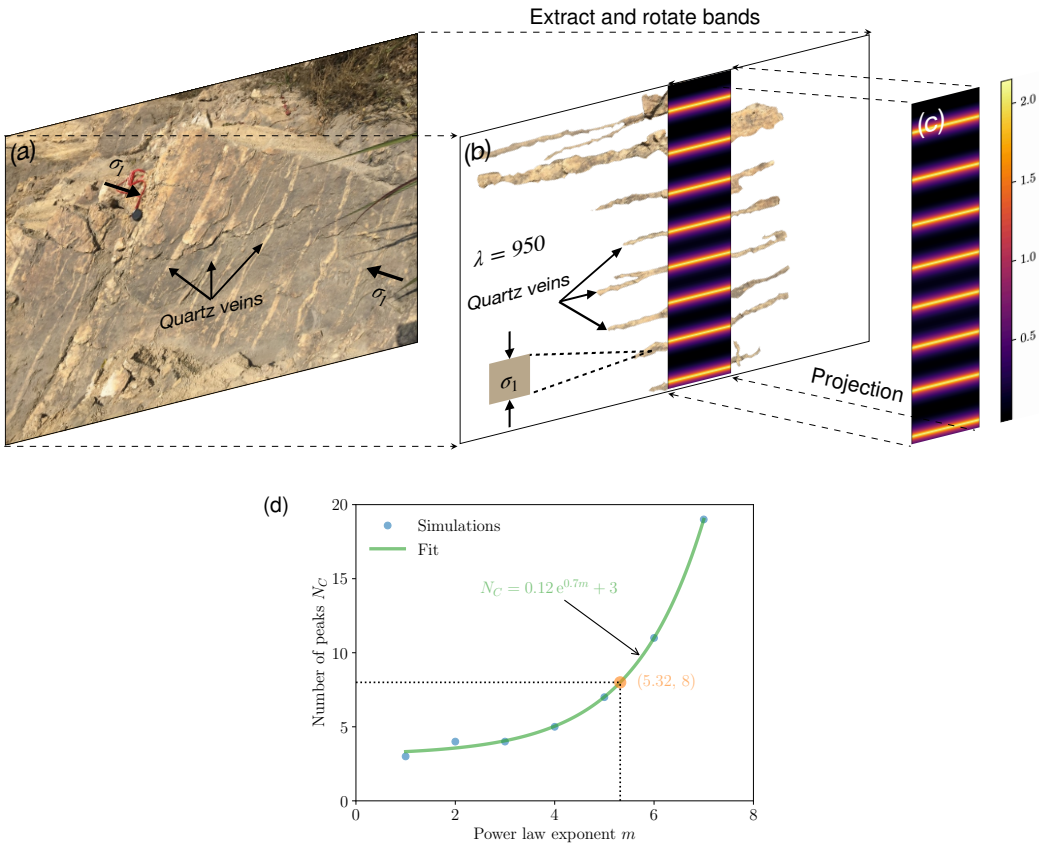


**Figure 3.** Reproducing quartz veins' patterns in the field using the proposed cnoidal wave-driven fracturing mechanism: (a) the potential stress state leads to compaction bands in quartz veins, (b) comparison of cnoidal wave-driven model and quartz veins in the field, (c) ASFEM simulations of the cnoidal wave propagation inducing compaction bands, and (d) effect of the rate-independent exponent $m$ on the number of stress singularities.

ture in conjunction with crystal growth justifies the simplified local equilibrium assumption of creeping flow between solid- and fluid-mass exchange. This cnoidal-induced instability combined with quartz dissolution-precipitation offers a new mechanism to describe quartz vein formation.

Quartz veins segment the host rock into almost equal spacing $h$, as Figure 3(a) illustrates. The minor deviation of the spacing $h$ may come from the heterogeneous material properties, or other effects. As demonstrated in Section 3.1, the spacing $h$ is significantly affected by the poromechanical parameter $\lambda$ as Figure 2(a) depicts.

We use the spacing to estimate the ratio $\lambda$ by reproducing the spacing between the quartz veins in the field observation. We find eight quartz veins observed in the field image, which corresponds to the value of $\lambda = 950$, as shown in Figure 3(b). Our numerical solution can reproduce the quartz veining by the corresponding cnoidal waves as shown in Figure 3(c). For this comparison, we have extracted and rotated the field image and then projected the numerical solutions into this image. Figure 3(b) compares the field observations and numerical solutions.

**Table 1.** Material parameter values for cataclasites under high-temperature conditions.

| Parameter | Symbol | Units | Value | Ref. |
|---|---|---|---|---|
| Permeability | $k$ | [m$^2$] | $10^{-15}$–$10^{-18}$ | Carpenter et al. (2014) |
| Fluid viscosity | $\mu_f$ | [Pa·s] | $10^{-4}$ | Cornelio et al. (2019) |
| Solid viscosity | $\mu_s$ | [Pa·s] | $10^{9}$ | Prival et al. (2022) |
| Applied overstress | $\bar{p}_n$ | [Pa] | - | Estimated |
| Strain (loading) rate | $\dot{\varepsilon}_n$ | [s$^{-1}$] | $10^{-10}$–$10^{-9}$ | Hu et al. (2021) |
| Bands' spacing | $h$ | [m] | 0.125–0.5* | Estimated |
| Rate-dependent coefficient | $m$ | [-] | 1–7 | Geomaterials |

* The values are estimated by the data from Tannock, Herwegh, Berger, Liu, and Regenauer-Lieb (2020), where 2–8 bands appear in an unit length.

Finally, to further justify our estimated value of $\lambda = 950$, we can evaluate the possible range of the poromechanical parameter by the following formula:

$$\lambda = \frac{\mu_f}{k\mu_s} h^2 N_C^2 \tag{3}$$

where the fit is compared to typical material properties found in the literature for cataclasites under high-temperature environments, as listed in Table 1, we set the stress numbers to $N_C = 8$. Accordingly, we can compute the reasonable value $\lambda$ in the 100 to $1.6\times 10^6$ range. The minimum value $\lambda = 100$ is over the critical points $\lambda = 12.7$ for the appearance of stress singularity, and this range contains the estimated $\lambda = 950$ for the quartz veins in the field. This justifies the working hypothesis that the cnoidal wave theory is a mechanism that can be used for inverting the poromechanical parameter by reproducing rhythmic mineralized patterns, for example, quartz veins.

### 3.4 Regularizing rate-dependency of geomaterials

Numerical simulations enable us to estimate the rate-dependent coefficient $m$ for porous rocks, which relates to the evolution of the plastic strain rate beyond the initial yield point, also known as Perzyna overstress plasticity (Perzyna, 1966). Unlike the linear rheology relationship $m = 1$ proposed for a partially molten rock (McKenzie, 1985), metamorphic compaction rates may induce nonlinear viscous rheology for porous rocks in which the rate-dependent coefficient $m > 1$. However, the parameter is hard to constrain for two reasons. First, in-situ measurements of the rheology remain an impossible task for the upper crust of Earth. Second, although the analytical solution has been proposed by Regenauer-Lieb et al. (2013) for integer exponent numbers $m = 1, 2, 3$, geomaterials are likely to have a higher order of expansion or non-integer (Hickman & Gutierrez, 2007; Oka et al., 2011). Therefore, as we assumed a widely used quantity $m = 3$ for quartz veins formation in the foregoing analysis, it may differ for realistic granitic rocks in high-temperature environments. However, the limitations can be resolved by the numerical method we developed.

In the following, we shall emphasize that the rate-dependent coefficient can be derived for the same quartz veins patterns shown in Figure 3(a). To achieve this, we first select the possible quantity of $\lambda = 240$ from the estimated range in Section 3.3. We then vary $m$ values ranging from 1 to 7 with the unit increment and investigate the effect of $m$ on the number of stress singularities. Figure 3(d) plots an exponential curve fitting the varied $m$ with the corresponding stress peaks, and its formula reads:

$$N_C = 0.12 \exp(0.7m) + 3 \tag{4}$$

After obtaining this relationship, we can derive the corresponding rate-dependent coefficient as $m = 5.32$ by substituting $N_C = 8$ into (4). To confirm the accuracy of our estimation, we input the parameter $m = 5.32$ and perform the simulation again. We observe eight stress peaks in our numerical simulation. The whole profile agrees with the field image. This example demonstrates that the combination of $m = 5.32$ and $\lambda = 240$ gives similar patterns observed in the quartz veins, indicating that we should account for the influence of the rate-dependent exponent of the power-law rheology. A higher exponent than expected from laboratory creep laws of granite implies the cataclasites of a more highly nonlinear deformation process, which could be a brittle micromechanism that is not unexpected at the brittle-ductile transition.

### 3.5 Potential to derive geological information

The analysis of mineralized patterns using the cnoidal wave theory provides the potential to derive from geological information in the field in-situ properties such as the solid viscosity $\mu_s$ and the overstress acting on the matrix for the mesothermal brittle-ductile conditions. The complex geological conditions are hard to achieve in laboratory experiments, e.g.the background strain rates, tectonic stress, temperature, and pressure, making the solid viscosity challenging to constrain. As an alternative method, we propose to reproduce the mineralized patterns by our numerical approach and invert the poromechanical parameter $\lambda$, thereby determining the solid viscosity in the following form:

$$\mu_s = \frac{\mu_f}{k\lambda} h^2 N_C^2 \tag{5}$$

We estimate the parameter $\lambda = 950$ by matching the quartz vein pattern, which can be substituted into (5). The solid viscosity is constrained in the range of $1.68\times10^9$–$10^{12}$ Pa·s with $h = 0.5$ m. Furthermore, if the strain rate can be measured (here, we adopt $10^{-9}$ s$^{-1}$ by Hu et al. (2021)), we can estimate the overstress during instabilities by $\bar{p}_n = \dot{\varepsilon}_n \mu_s$, which for the Heyuan Fault example is surprisingly small between 1.68 and 1680 Pa above the yield stress. Given the uncertainty in the effect of the power law exponent and the $\lambda$ ratio, we conclude that the required overstress for the observed spacing in the shown field example is 1–2000 Pa. This suggests that strain localization can be formed under low geological loading rates and low overstress levels in mesothermal crust conditions. Cnoidal wave theory suggests that large-scale mineralization events are inferred to be not a result of a short catastrophic event but a result of prolonged tectonic periods at relatively low overstress levels. This alleviates the problem of demanding high fluxes of metamorphic fluids at higher than lithostatic fluid pressures required by the alternative fault-valve or crack-seal mechanisms.

## 4 Conclusion

This paper offers a fresh look at mineralization patterns related to metamorphic breakdown reactions in a tectonically stressed environment. The cnoidal wave theory in solids is a possible candidate to explain the formation of mineral deposits in mesothermal quartz veins. We conclude that a plausible new mechanism for mineralizing systems has been developed based on the cnoidal wave instabilities theory. The new approach extends the classical fault valve hypothesis by an alternative cnoidal wave hypothesis and allows for explaining the repeated mineralized patterns under compressive conditions. Although the cnoidal wave theory allows analytical solutions, we have shown the advantage of extending the solution by the adaptively stabilized finite element method (ASFEM) to capture cnoidal wave-driven stress singularities appearing in mineralizing systems. The ASFEM provides a flexible and effective way to reproduce the mineralization patterns compared to the analytical theory. The analytical solution is simplified and only allows considering an integer rate-dependent coefficient $m \leq 3$. The numerical model presented here can overcome this limitation.

We emphasize that the approach should be considered as a first pilot study since the application of the cnoidal wave theory to the geological case study of mineralizing vein formation is not yet an accepted model. This would require detailed geological follow-up case studies constrained by barometry, thermometry, microstructural analyses, fluid inclusion studies, chemical analysis, and tectonic field studies, which are beyond the scope of this contribution. In this study, we have shown that our numerical approach provides an effective method to invert the rheological parameters and diffusion ratios accurately under in-situ conditions, which are hard to estimate in experiments or evaluate by analytical theories.

## 5 Open Research

The data are available on Mendeley Data (Liu et al., 2023c).

**Acknowledgments**

The authors thank Roberto J. Cier for providing the ASFEM code. The support of the Research Grant Council of Hong Kong (ECS 27203720 and GRF 17206521) and the Australian Research Council (ARC DP200102517, DP170104550, LP170100233) is acknowledged.

## References

Alevizos, S., Poulet, T., Sari, M., Lesueur, M., Regenauer-Lieb, K., & Veveakis, M. (2017). A framework for fracture network formation in overpressurised impermeable shale: deformability versus diagenesis. *Rock Mechanics and Rock Engineering*, *50*, 689–703.

Barker, R. D., Barker, S. L., Wilson, S. A., & Stock, E. D. (2021). Quantitative mineral mapping of drill core surfaces I: a method for $\mu$XRF mineral calculation and mapping of hydrothermally altered, fine-grained sedimentary rocks from a Carlin-type gold deposit. *Economic Geology*, *116*(4), 803–819.

Bons, P. D., Elburg, M. A., & Gomez-Rivas, E. (2012). A review of the formation of tectonic veins and their microstructures. *Journal of Structural Geology*, *43*, 33–62.

Carpenter, B., Kitajima, H., Sutherland, R., Townend, J., Toy, V., & Saffer, D. (2014). Hydraulic and acoustic properties of the active Alpine Fault, New Zealand: Laboratory measurements on DFDP-1 drill core. *Earth and Planetary Science Letters*, *390*, 45–51.

Chen, J., Tang, X., & Hu, M. (2023). Shear instability in geothermal fields under hydromechanical feedback. *Geophysics*, *88*(5), 1–56.

Chen, R., Lindqwister, W., Wu, F., Mielniczuk, B., Hueckel, T., & Veveakis, M. (2023). The physics of desiccation cracks 1: Ductile fracturing and dependence on relative humidity. *Geomechanics for Energy and the Environment*, 100488.

Cier, R. J., Labanda, N. A., & Calo, V. M. (2022). Compaction band localization in geomaterials: a mechanically consistent failure criterion. *arXiv preprint arXiv:2202.03849*.

Cier, R. J., Poulet, T., Rojas, S., Veveakis, M., & Calo, V. M. (2021). Automatically adaptive stabilized finite elements and continuation analysis for compaction banding in geomaterials. *International Journal for Numerical Methods in Engineering*, *122*(21), 6234–6252.

Cornelio, C., Spagnuolo, E., Di Toro, G., Nielsen, S., & Violay, M. (2019). Mechanical behaviour of fluid-lubricated faults. *Nature Communications*, *10*(1), 1274.

Hickman, R., & Gutierrez, M. (2007). Formulation of a three-dimensional rate-dependent constitutive model for chalk and porous rocks. *International Journal for Numerical and Analytical Methods in Geomechanics*, *31*(4), 583–605.

Hobbs, B., & Ord, A. (2022). Failure modes in fluid saturated rocks: deformation processes and mode-switching. *Geological Magazine*, *159*(11-12), 2002–2019.

Hobbs, B., & Ord, A. (2023). An alternative to the fault-valve model. *Australian Journal of Earth Sciences*, 1–14.

Hu, J., Yu, X., Li, W., He, Y., Liu, N., & Zhang, Y. (2021). Structural and rheological features of the northeastern Sanyang shear zone in the eastern Jiangnan orogen: Indications for early Paleozoic orogeny in the South China Block. *Journal of Structural Geology*, *153*, 104472.

Issen, K. A., & Rudnicki, J. W. (2000). Conditions for compaction bands in porous rock. *Journal of Geophysical Research: Solid Earth*, *105*(B9), 21529–21536.

Kelka, U., Veveakis, M., Koehn, D., & Beaudoin, N. (2017). Zebra rocks: compaction waves create ore deposits. *Scientific Reports*, *7*(1), 1–9.

Liu, C., Calo, V., Regenauer-Lieb, K., & Hu, M. (2023a). Coefficients of reaction-diffusion processes derived from patterns in rocks. *Journal of Geophysical Research: Solid Earth*, *128*(5), e2022JB026253.

Liu, C., Calo, V., Regenauer-Lieb, K., & Hu, M. (2023b). Dendritic growth patterns in rocks: Inverting the driving and triggering mechanisms. *Journal of Geophysical Research: Solid Earth*, *128*, e2023JB027105.

Liu, C., Calo, V., Regenauer-Lieb, K., & Hu, M. (2023c). *A new mechanism for mineralizing systems based on cnoidal wave instabilities* [Dataset]. Mendeley Data. Retrieved from `https://data.mendeley.com/datasets/szz3j7kgc8/1` doi: 10.17632/szz3j7kgc8.1

McKenzie, D. (1985). The extraction of magma from the crust and mantle. *Earth and Planetary Science Letters*, *74*(1), 81–91.

Oka, F., Kimoto, S., Higo, Y., Ohta, H., Sanagawa, T., & Kodaka, T. (2011). An elasto-viscoplastic model for diatomaceous mudstone and numerical simulation of compaction bands. *International Journal for Numerical and Analytical Methods in Geomechanics*, *35*(2), 244–263.

Perzyna, P. (1966). Fundamental problems in viscoplasticity. *Advances in Applied Mechanics*, *9*, 243–377.

Prival, J.-M., Harris, A. J., Zanella, E., Robustelli Test, C., Gurioli, L., Chevrel, O., & Biren, J. (2022). Emplacement dynamics of a crystal-rich, highly viscous trachytic flow of the Sancy stratovolcano, France. *Geological Society of America Bulletin*.

Ramsay, J. G. (1980). The crack–seal mechanism of rock deformation. *Nature*, *284*(5752), 135–139.

Regenauer-Lieb, K., Poulet, T., & Veveakis, M. (2016). A novel wave-mechanics approach for fluid flow in unconventional resources. *The Leading Edge*, *35*(1), 90-97.

Regenauer-Lieb, K., Veveakis, M., Poulet, T., Wellmann, F., Karrech, A., Liu, J., ... others (2013). Multiscale coupling and multiphysics approaches in earth sciences: Applications. *Journal of Coupled Systems and Multiscale Dynamics*, *1*(3), 281–323.

Sibson, R. H., Robert, F., & Poulsen, K. H. (1988). High-angle reverse faults, fluid-pressure cycling, and mesothermal gold-quartz deposits. *Geology*, *16*(6), 551-555.

Späth, M., Urai, J. L., & Nestler, B. (2022). Incomplete crack sealing causes localization of fracturing in hydrothermal quartz veins. *Geophysical Research Letters*, *49*(15), e2022GL098643.

Tang, X., & Hu, M. (2023). A reactive-chemo-mechanical model for weak acid-assisted cavity expansion in carbonate rocks. *Rock Mechanics and Rock Engineering*, *56*(1), 515–533.

Tannock, L., Herwegh, M., Berger, A., Liu, J., Lanari, P., & Regenauer-Lieb, K. (2020). Microstructural analyses of a giant quartz reef in south China reveal episodic brittle-ductile fluid transfer. *Journal of Structural Geology*, *130*,

103911.

Tannock, L., Herwegh, M., Berger, A., Liu, J., & Regenauer-Lieb, K. (2020). The effects of a tectonic stress regime change on crustal-scale fluid flow at the Heyuan geothermal fault system, South China. *Tectonophysics*, *781*, 228399.

Tomkins, A. G. (2013). On the source of orogenic gold. *Geology*, *41*(12), 1255–1256.

Veveakis, E., & Regenauer-Lieb, K. (2015). Cnoidal waves in solids. *Journal of the Mechanics and Physics of Solids*, *78*, 231–248.

Veveakis, E., Regenauer-Lieb, K., & Weinberg, R. (2014). Ductile compaction of partially molten rocks: the effect of non-linear viscous rheology on instability and segregation. *Geophysical Journal International*, *200*(1), 519–523.

Weinberg, R. F., Veveakis, E., & Regenauer-Lieb, K. (2015). Compaction-driven melt segregation in migmatites. *Geology*, *43*(6), 471–474.

## References From the Supporting Information

Coussy, O. (2004). *Poromechanics*. John Wiley & Sons.

Hill, R. (1962). Acceleration waves in solids. *Journal of the Mechanics and Physics of Solids*, *10*(1), 1–16.

Kohlstedt, D., Evans, B., & Mackwell, S. (1995). Strength of the lithosphere: Constraints imposed by laboratory experiments. *Journal of Geophysical Research: Solid Earth*, *100*(B9), 17587–17602.

Perzyna, P. (1966). Fundamental problems in viscoplasticity. *Advances in Applied Mechanics*, *9*, 243–377.